

Topological Analysis of Cancer Cell Structures Simulated in MATLAB for Radiation Dosage Calculation and Optimization

Miel Gabriel Lagdan,^{a,*} and Rosmond Jae Punzalan^a

^a*College of Arts and Sciences, University of the Philippines Manila*

*Corresponding author: mlagdan@up.edu.ph

1 Introduction

Cancer remains prevalent among the population, cited as the leading cause of death worldwide, with metrics insisting one in six deaths are due to cancer-related complications. Statistics from GLOBOCAN from their analysis of cancers in 2022 report nearly 20 million new instances of cancer worldwide with an associated number of deaths from cancer amounting to around 9.7 million [1].

To combat the threat cancer imposes on global health, national institutes of countries and other institutions invested in research for the pursuit of advancements in oncology, which led to the development of numerous available cancer treatments in the world, some more sophisticated, some more dangerous than others.

Radiation therapy, also known as radiotherapy, is a type of cancer treatment procedure utilizing ionizing radiation to kill cancerous cells in a patient's body [2]. Depending on the type of cancer, a specific ionizing radiation type and dosage will be given to the patient. However, it must be noted that radiotherapy has its own limitations. Cells, specifically cancer cells, have specific radioresistances, either innate or acquired. Radioresistance is defined as the ability of the cell to withstand and resist the effects of radiation, and from the degree or strength of the cell's radioresistances, it can hinder the implementation of radiation therapy [3].

One of the classical methods in assessing cancer cell response, their radioresistances and radiosensitivities, and evaluating the efficacy of the radiation therapy is through clonogenic assay tests. Clonogenic assay tests measure a single cell's ability to form colonies [4]. This procedure quantitatively measures the effect of the radiation to the target cell. However, the number of colonies formed by the cell alone does not account for the other factors affecting the radioresistances and radiosensitivities of the cancer cells.

This includes the ability of the cell to form structures that may affect its resistance to the incoming radiation. Additionally, how the cells are linked to one another forming one single colony may also affect the amount of radiation that must be exposed to the target. These unaccounted factors may affect the optimal radiation dosage that will be given to the target cancer cell, resulting in an inefficient radiation exposure to the patient. Hence, the need to perform studies using topological analysis.

One study [5] utilized topological analysis in measuring the radioresistivity of lung cancer cell lines by examining the 2D cell networks for a single colony and observing its cell graph topology. It is found that the clustering network of the cell has an effect on its radiosensitivity upon the exposure to the radiation dose. Additionally, from the results of the study, it was suggested that topology can be another method of quantitatively measuring and examining radiosensitivities of cancer cell lines, allowing for the assessment of the performance of radiation therapy.

However, a problem still persists in many countries in the world. Resource disparity inhibits production of more efficient, effective, and tailored treatment regimes for cancer especially in the developing countries. This makes a simple yet powerful cancer-radiation model vital for treatment planning in treatment centers, as low-cost resources become present, and sometimes necessitated for low-income populations. This cancer-radiation model, in this study, will be made in MATLAB, where Monte Carlo simulations are utilized to simulate photon treatment for the cancer cells. Morphological characteristics will then be examined in the same software.

This study aimed to provide a model of various cancer cell structures, allowing for the efficient and accurate calculation and optimization of radiation dosages, using topological analysis and Monte Carlo simulation. Specifically, this study aimed to

1. create a cancer-radiation model with different cancer cell structures in 2D that will be utilized in a radiation therapy simulation,
2. simulate different radiotherapy levels for every cancer structure that will be made, and
3. produce topological metrics and conduct analysis from the simulation.

Sec. 2 discusses the methods used in both the creation of the cancer-radiation model (Sec. 2.1 & 2.2) and analysis used (Sec. 2.3, 2.4). Sec. 3 and Sec. 4 discusses the results of the simulation and its implications.

2 Methodology

This project utilized MATLAB in order to create 2-dimensional cancer cell structures, perform a Monte

Carlo simulation of irradiating the created cells using photons, and analyze topologically how the 2D structures, focusing on the network systems of cancer cell colonies, affect the optimal amount of dose that must be given to the target cells.

2.1 2D Cancer Cell Structure Creation

Three main factors were considered during the creation of the 2D cancer cell structures, namely cell attenuation, radiosensitivity, and radioresistivity.

A value of 0.2 or 20% cell attenuation was set for the simulation. This allows the generated cancer cells to have low shielding in the inner regions and sufficient shielding on the outer parts against the incoming radiation. For the case of the radiosensitivity and radioresistivity, the Linear-Quadratic Model (LQM) model was utilized. The model uses the formula

$$S = e^{-\alpha D - \beta D^2} \quad [1]$$

, where α refers to cell death caused by single hit events and β refers to cell death caused by double or multiple hit events, hence the term Linear-Quadratic Model [6].

The project simulated 2 cases of the generated cancer cell colonies, one for head and neck cancer, an aggressively proliferating tumor, and one for prostate cancer, a slowly proliferating tumor. Table 1 displays various α , β , and α/β ratios of specific cancer cell lines from related literature and generated cancer cells used for the simulations.

Tumor Type	α	β	α/β
Head & Neck Cancer [7]			8.3-12.4
Prostate Cancer [8]			1.5-3
Aggressive Tumor	0.15	0.015	10
Slowly Proliferating Tumor	0.04	0.025	1.6

Table 1: Table of α, β for different tumors.

Other factors including the size of the cell colony, number of simulations, and the net threshold for the cell networks were included. The size of the cancer cell colony was set to 150. The number of Monte Carlo simulations set were 50. Lastly, the net threshold to consider adjacent colonies as part of the network was set to 20 pixels.

2.2 Cancer Cell Irradiation Simulation

The project simulated photon therapy, performing a Monte Carlo simulation of photon particles irradiating the generated cancer cell colonies. Varying dose values of photon radiation was utilized for the simulation, starting from 0 Gy up to 16 Gy with increments of 2.

Additionally, the cancer cell colonies were set to be located 4 cm deep into a 10 cm thick simulated tissue.

2.3 Data Collection

The simulation, given the factors and conditions involved, was performed for both types of tumors. The topology of the cancer cell colony at every dose given was processed and displayed. Additionally, the depth

vs. dose graph, particle fluence, pre and post radiation networks, and dose vs. fragmentation graph was also presented upon the collection of data from the simulation.

2.4 Topological Analysis

The framework used in conducting the topological analysis was laid out in a study by Tirinato [5]. Using MATLAB, the following topological metrics are calculated for the colonies formed:

1. *Clustering coefficients (cc)* - a measure of the degree to which nodes (cells) in a graph tend to cluster together. The local clustering coefficient is calculated by

$$C_i = \frac{2E_i}{k(k-1)} \quad [2]$$

wherein k is the number of neighbors of a generic node i , E_i is the number of existing connections between those, and $k(k-1)$ is the maximum number of connections, or combinations, that can exist among k nodes

2. *Characteristic path length (cpl)* - a measure of the average path length between each node (cells).
3. *Small world coefficients (sw)* - the ratio of the clustering coefficient (normalized by that expected in a random graph) to the average shortest path length (also normalized by that expected in a random graph).

The cells' morphology were also examined before and after bombardment, following measurements of their average area, eccentricity, and roundness to see the effect of radiation.

3 Results

The Monte Carlo simulation was performed for the 2 generated cancer cell types, namely the aggressive tumor and the slowly proliferating tumor. After 15 runs, the program generated the results for each of the factors and metrics being studied. The succeeding figures, graphs, and data shows the behavior and response of the two types of cancer cell colonies upon exposure to varying levels of photon radiation.

3.1 Radiation Dose vs. Depth

Figures 1a and 1b presents the dose vs. depth relation between the bombarded photon and the tissue it penetrated for both the aggressive and slowly proliferating tumor. The graph for both showed a sharp spike or a high entry energy deposition as the photon penetrated through the simulated tissues. This spike occurred at a depth less than 1 cm. After reaching the peak of energy deposition, the graphs displayed an exponential decay with the energy being deposited to the tissue as the photon traversed deeper to the tissue. The tumor/cancer cell colonies located 4 cm deep the tissue received a relative energy deposition value between 0.5 and 0.6 or about 50%-60%, similar to both types of tumors generated.

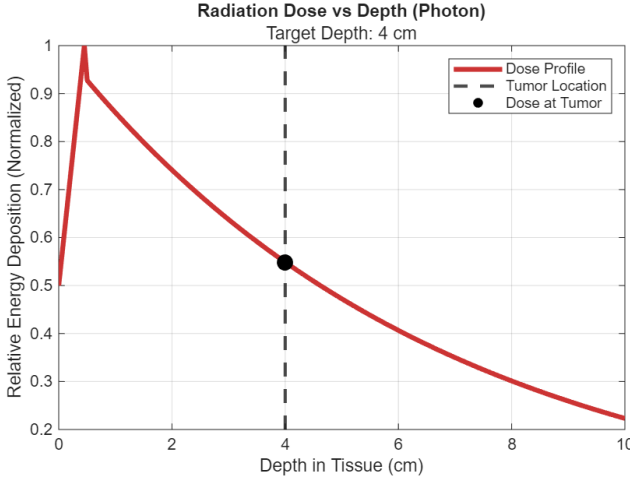


Figure 1a: Photon radiation dose vs. tissue depth graph for an aggressive tumor.

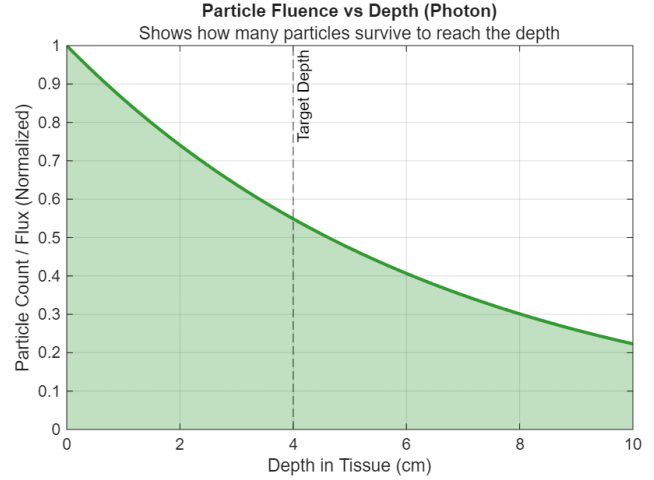


Figure 2a: Photon particle fluence vs. tissue depth for an aggressive tumor.

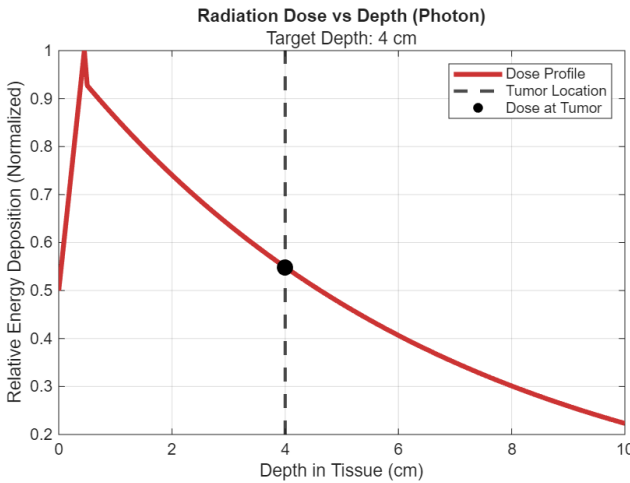


Figure 1b: Photon radiation dose vs. tissue depth graph for a slowly proliferating tumor.

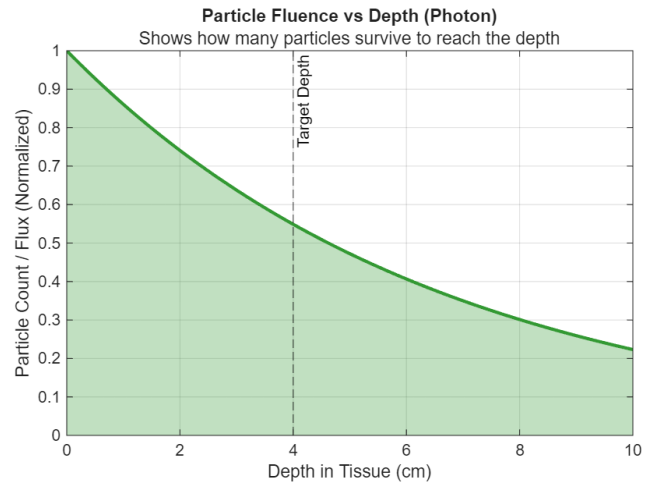


Figure 2b: Photon particle fluence vs. tissue depth for a slowly proliferating tumor.

3.2 Particle Fluence vs. Depth

Figure 2a and 2b presents the particle fluence vs. depth relation between the photons and the simulated tissue containing the generated tumors. The graphs show the normalized particle count or fluence at varying tissue depth. The colored region shows the surviving cancer cell population while the uncolored region displays the cancer cell population that died upon exposure to radiation. The graphs display an exponential decay as the particle went deeper into the tissue. It can be seen that at the tumor location, which is at 4 cm, the particle count is about 0.55 or 55% of the initial cancer cell population, for both aggressive and slowly proliferating/indolent tumor.

3.3 Radiation-Induced Network Topology Changes

Figure 3a and 3b displays the changes with the cancer cell colonies upon exposure to varying energy levels of radiation. Both types of tumor experienced a decrease in the number of black dots or circles as the radiation dosage increased. Clustering of the dots also changed as the radiation dosage given is modified. Less cluster-

ing was observed at higher doses, while more clustering and clumping was observed as lower doses up to 0 Gy.

Comparing the two images, it can be seen that at lower radiation dosages, the dots are darker for Fig. 3b (indolent) than for Fig. 3a (aggressive). At higher radiation dosages, both tumors displayed similar behaviors in response to the radiation. The number of dots greatly decreased for both, however, the number of dots that remained after irradiation was slightly greater for the indolent tumor than the aggressive tumor.

3.4 Colony Networks and Fragmentation

Figures 4a and 4b displays the networks formed before and after exposing the cancer cell colonies to various levels of radiation. Cancer cell colonies separated by a distance of at most 20 pixels are considered as part of the network, while overlapping cell colonies are considered part of a single cell colony. For both types of tumors, it can be observed that the amount of networks formed increased post-radiation compared to the networks present pre-exposure to radiation, as seen by the number of connections between the cell colonies in the diagram.

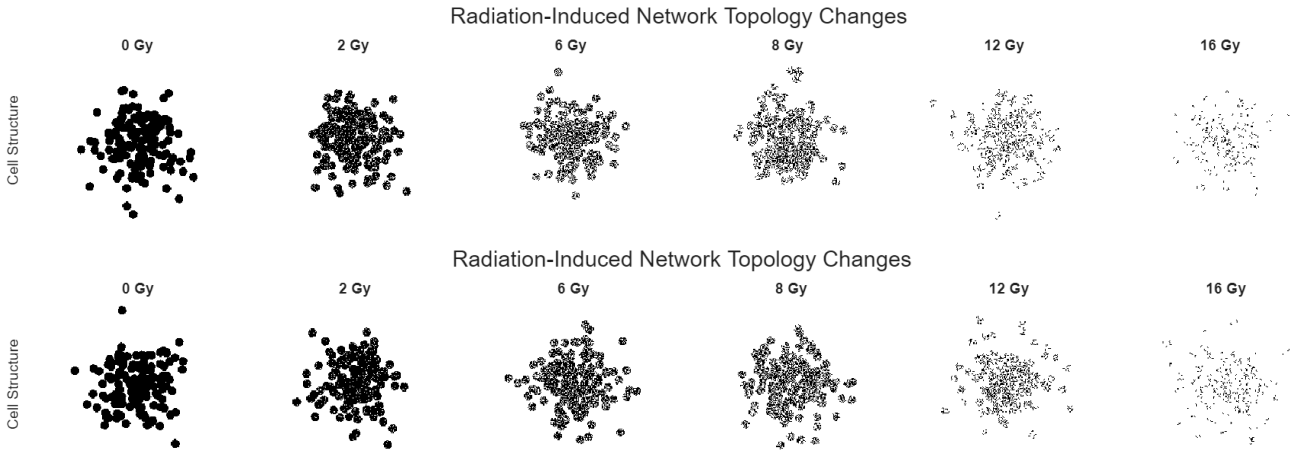


Figure 3: Evolution of the tumor's network topology under radiation for an (a) aggressive tumor (top) and a (b) slowly proliferating tumor (bottom).

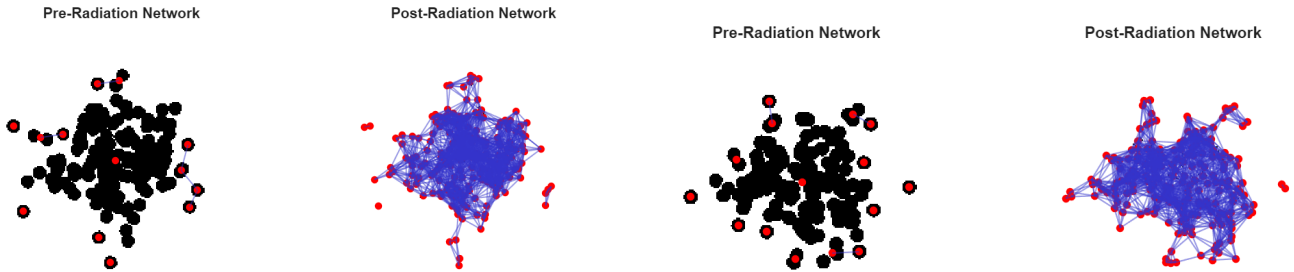


Figure 4: Pre and post radiation networks within the (a) generated aggressive tumor (left) and (b) generated slowly proliferating tumor (right).

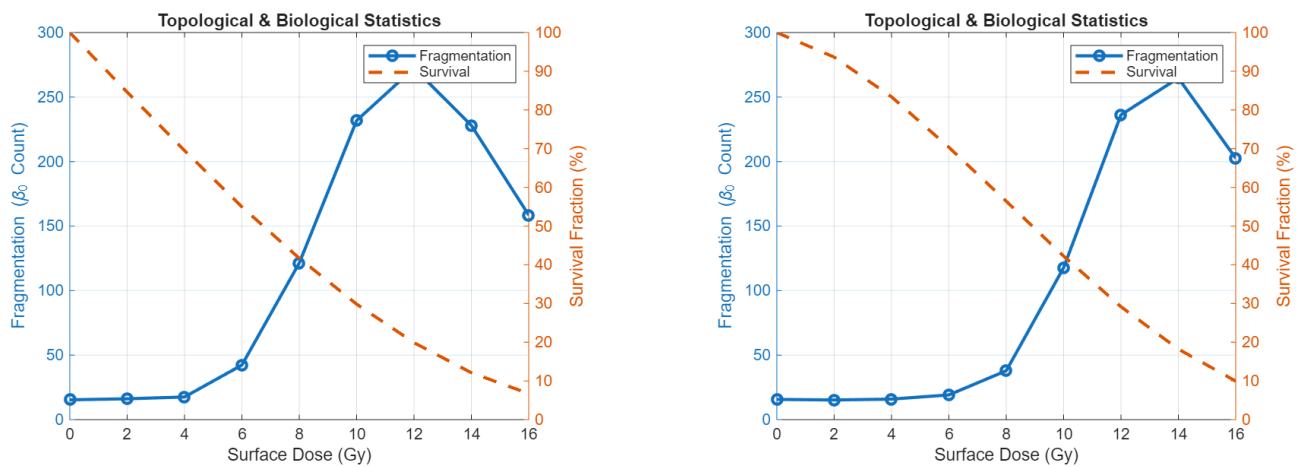


Figure 5: Fragmentation vs. radiation dosage for (a) an aggressive tumor (left) and (b) a slowly proliferating tumor (right).

Figures 5a and 5b on the other hand, displays the tumor fragmentation vs. radiation dosage relationship, presenting how the amount of dose given to the tumor affects how radiation breaks down big cancer cell colonies to smaller groups. Fig. 5a displays a seemingly exponential graph, where fragmentation increased when dosage values are increased from 0 Gy to 12 Gy, then continuously dropped when dosage was further increased. Fig. 5b also displayed the same exponential increase then drop after the peak, similar to Fig. 5a. The difference between the two is that at lower radiation doses, the slowly proliferating tumor experienced less fragmentation than the aggressive tumor. The peak of fragmentation also differs between the two cancer types, 12 Gy for the aggressive tumor and 14 Gy for the slowly proliferating tumor.

3.5 Cancer Cell Topology Metrics

Figures 6a and 6b displays the graphs of the metrics measured in relation to the topology of the generated cancer cell colonies. The clustering coefficients, characteristic path lengths, and the small-world coefficient are measured. Moreover, Figures 7a and 7b displays the other factors relating to cancer cell structures, namely mean node eccentricity, mean area, mean parameter, and mean roundness was also measured.

For the case of the aggressive tumor, the clustering coefficient showed a slight decrease then a sharp increase of values at the lower radiation dosages before maintaining a relatively constant trend beyond 10 Gy. The characteristic path length displayed a fast increase in values, peaking at 4.5 cpl at around 7 Gy before its value dropped. The small-world coefficient on the other hand, exhibited a similar trend of sharply rising in values, peaking at 4 sw at around 7 Gy, and eventually decreasing in value but at a slower pace unlike in the characteristic path length. For the metrics measured for the cancer cell structures, both the mean area and mean perimeter showed a great drop in values as the radiation dose increased. The mean roundness on the other hand increased in values as the dose increased. Lastly, the mean node eccentricity exhibited a sharp increase at the lower radiation dosages then eventually dropped then stabilized at radiation doses beyond 10 Gy.

For the case of the slowly proliferating tumor, the trends for both graphs of the topological and geometric measurements/metrics are relatively similar to the behavior of the graphs for the aggressive tumor. The clustering coefficient shows a fast increase at the lower dosages then peaked at around 10 Gy. The clustering coefficient then stabilizes at radiation doses beyond 10 Gy. The characteristic path length showed a sharp increase near 10 Gy then peaked at the said dosage value. The characteristic path length then drops significantly at the higher dosages. The small-world coefficient on the other hand showed a stable increase at the lower dosages, peaked at around 10-12 Gy, then continuously decreased as the dosage values increased. For the metrics used for the cancer cell structures, both the mean area and mean perimeter showed a great decrease in

value as the dosage of radiation increases. The mean roundness showed an increase as the radiation dose also increased. Lastly, the mean node eccentricity displayed a sharp increase at the lower dosages, peaked at 10 Gy, and then showed a great decrease in values as radiation doses exceed beyond 10 Gy.

4 Discussion

The study was able to provide a cancer-radiation simulation setup that was able to provide reliable network topology changes depicting cell survival and quantifiable morphological and topological metrics that are similar to experimental setups conducted by studies [5].

4.1 Topology Changes and Cell Death

Figures 3a and 3b depict cells, represented by black dots, and their survival after application of different dosages of photon radiation (in Gy). We see a trend of decreasing cell survival as the dosage is increased, caused by irreparable DNA damage that makes the cells unable to sustain itself within the irradiated environment.

This measure of damage is denoted by the relative biological efficacy of radiation (RBE) which depends on the radiation energy, dose, and dose rate [9, 10] which can result from both direct and indirect action of radiation [11]. As both setups used the same dose rate (delivered almost instantaneously) and radiation energy, changes (and cell death) is mostly attributed to the changes incurred by the dose applied to each level.

This is a result expected to occur. Studies insist that cell death due to irradiating the cells with photons incurs DNA damage proportional to dose (proportional dose-response relationship) that cell cycle arrests in multiple cell cycle checkpoints occur (G2/M), leading to cell death and decreased cell proliferation [12–15].

Upon closer examination of the network topology changes between aggressive and slowly proliferating tumor types in fig. 3a and 3b respectively, darkness in the graphs (which indicate cell survival) is more prominent in the slowly proliferating type in lieu of the aggressive type when reaching around dosages 2-12 Gy.

This implies that proliferation rates also contribute to the survival of cancer cells. After all, the S (synthesis) phase within the cell cycle is a relatively radioresistant event. Studies demonstrate that slowly proliferating cells when applied with a dosage of radiation delays transition into the S phase and gets suspended along the transition of G1 and S phases. This leads to a relatively homogeneous makeup of cells which are within the same phase, in comparison to rapidly proliferating cells (aggressive), which consists of cells in relatively inhomogeneous cell cycle stages, making the cells more prone to being in phases which are less radioresistant [16, 17].

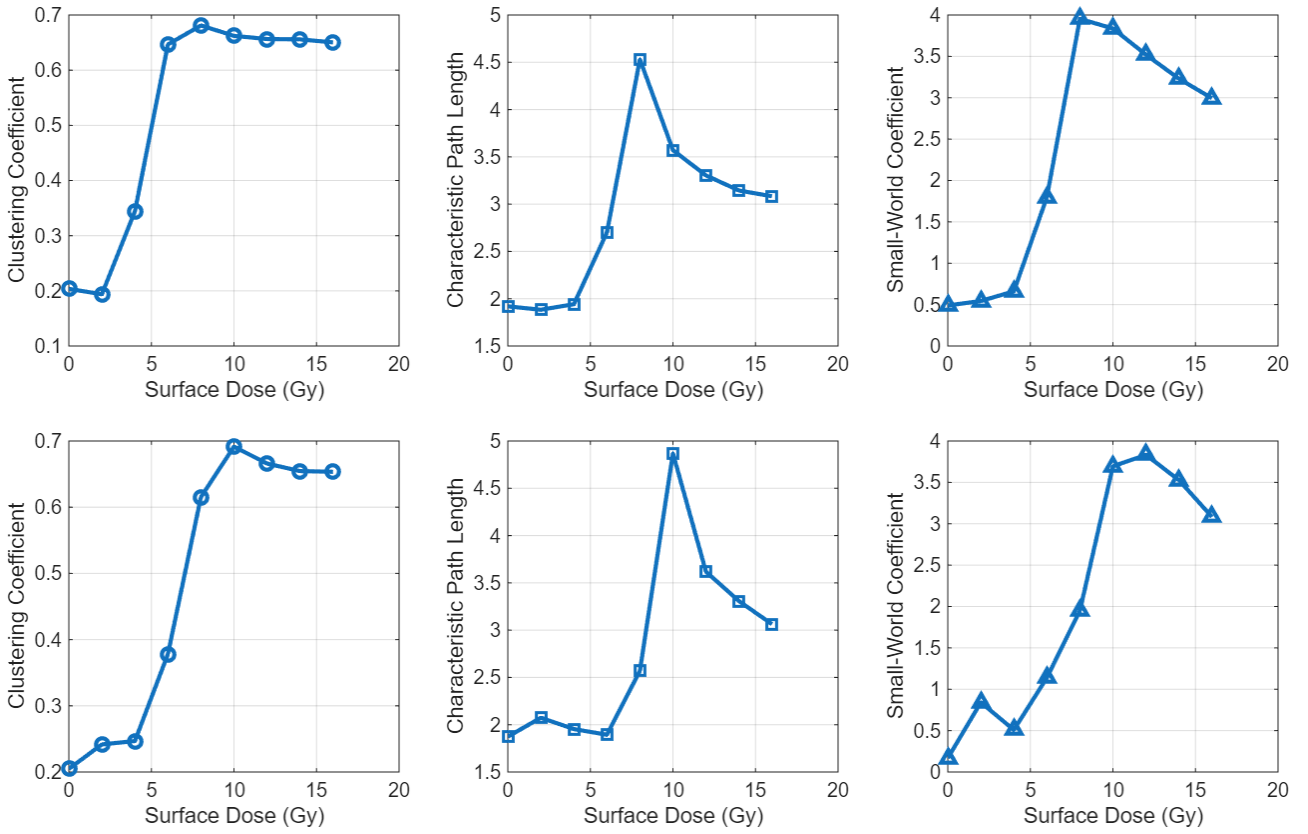


Figure 6: Cancer cell colonies topological metrics for (a) an aggressive tumor (top) and (b) a slowly proliferating tumor (bottom).

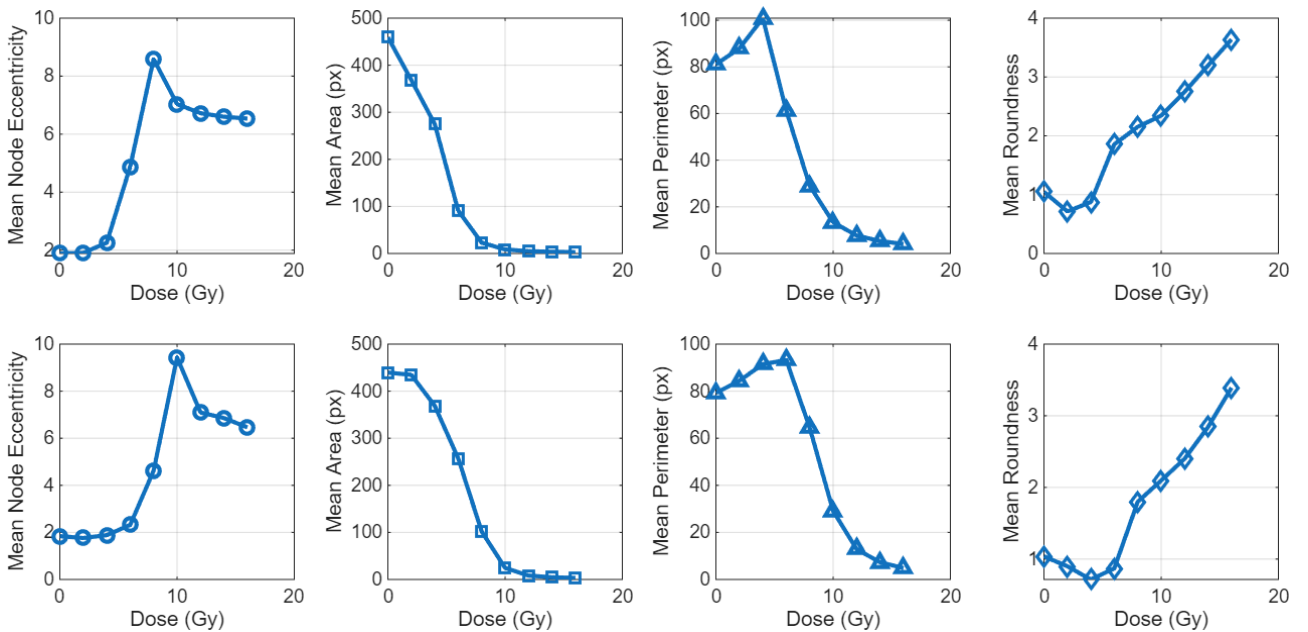


Figure 7: Cancer cell structure metrics for (a) an aggressive tumor (top) and (b) a slowly proliferating tumor (bottom).

4.2 Network Topology of Surviving Cells

Before and after application of radiation, a network was established using a deterministic ϵ -neighborhood graph with a hard interaction radius displayed in Fig. 4a and 4b.

The pre-radiation networks feature large radius black areas, which amass cancer cells in close proximity with each other which essentially makes them continuous. These large radii essentially represent one large mass of cells (not taking into account each individual cell). This is prevalent with the few centroids (red dots) and few connections present. The network nodes therefore represent connected cellular regions, not single cells, and edges encode spatial proximity between these regions.”

The post-radiation network, however, exhibits an increased number of centroids (red nodes) and inter-connecting edges (blue lines). The contiguous cellular masses present prior to radiation exposure fragment into multiple disconnected clusters, resulting in numerous centroids and proximity-based connections defined by the network threshold encoded in the model. This fragmentation is evidenced by the disappearance of large contiguous black regions and is attributed to radiation-induced cell death within the tumor mass, as discussed in Sec. 4.1.

At this stage, it is important to note that the apparent increase in network connectivity arises primarily from fragmentation rather than from the emergence of new cells. As large coherent cellular regions break down into smaller surviving clusters, each cluster becomes an independent network node capable of forming connections with neighboring clusters. Consequently, the network displays an implied increase in connectivity driven by reduced structural coherence and weakened cell-cell adhesion, rather than by an increase in cell number.

This network topology is best explained by the resulting computation and analysis of the clustering coefficient, characteristic path length, and small world coefficient.

4.3 Fragmentation vs. Survival

Fig. 5a and 5b depicts an approximately inverse relationship between fragmentation and survival of cells. Outside of this relationship, as explained by Sec. 4.1 and 4.2, application of the radiation dose led to both the death of cells (lessened survival) and fragmentation.

The graphs, however, show rapidly increasing fragmentation from increased dosage between 6-8 Gy (for rapidly proliferating) and 8-12 Gy (for slowly proliferating). After which, at higher doses after the aforementioned intervals, fragmentation seems to decrease. This behavior is consistent with a possible shift from controlled apoptotic events as a result of chromosomal damage to structural integrity effects to the cell body themselves.

Higher doses provide adequate energy to destabilize the cell structure leading to immediate cell death

(necrosis). Whereas cancer cells may be able to undergo repair by going through the cell cycle, high-dose application bypasses this by leading to immediate cell destruction [18]. This explains a higher tolerance of fragmentation in slowly proliferating cells (8-12 Gy), as they are more able to undergo repair in comparison to aggressive cells.

Some studies suggest that this fragmentation may also be a form of survival mechanism through metastasis. One study claims that their data shows that cell clustering induces a hypoxic environment, consistent with previous reports showing that tumor spheroids have hypoxic centers, leading to mitophagy associated with clearance of damaged mitochondria and improving cell survival [19]. In the context of the simulation however, as the cells are relatively static, this survival mechanism is not displayed, and survival remains roughly a negatively sloped graph.

Another study suggests that this fragmentation generates cell-associated debris which provide protective effects against cytotoxic drugs [20]. However, cytotoxicity is beyond the scope of this study as it only considers radiotherapeutic effects.

4.4 Small-world-ness

Small Worldness Topological metrics (clustering coefficient, characteristic path length, and then small world coefficient) were measured before and after application of the radiation with differing doses. The values are graphed given by Fig. 6a and 6b.

4.4.1 Clustering coefficient (cc)

The clustering coefficient measures how tightly nodes cluster together, the likelihood that neighbors of a node are also connected to each other. In our simulations, the clustering coefficient increases with radiation dose, showing a rapid rise between ~2-6.Gy for aggressive tumors and 5-10.Gy for slowly proliferating tumors. This suggests that more densely connected communities are forming in these dose ranges, meaning that neighbors of a node are more likely to be connected, forming “triangles.”

However, as discussed in Sec. 4.3, at these doses, cancer cells are also more prone to fragmentation, which seems counterintuitive to the notion of denser connectivity. As explained in Sec. 4.2, this can be understood by considering that initially, cells are densely packed into a large mass, which counts as one cluster. Radiation causes fragmentation of this mass, and the resulting smaller clusters appear as additional connections in the network. Thus, the observed increase in clustering coefficient reflects this fragmentation effect, making the trends reasonable over the specified dose intervals.

Eventually, at higher doses, the cc plateaus, indicating that cluster density eventually reaches a peak, at least for this simulation. This may be explained similarly to the phenomena explained in Sec. 4.3. At higher doses, fragmentation may occur less that more cells tend to undergo necrosis and undergo unorganized

destruction.

4.4.2 Characteristic path length (cpl)

The characteristic path length measures the average shortest path length in between centroids. Eventually, the graphs portray a peak characteristic path length achieved around ~ 8 Gy with cpl of ~ 4.5 for aggressive tumors and peak cpl around ~ 10 Gy with cpl of ~ 5 . This implies that slowly proliferating tumors have higher peak lengths upon fragmentation, however, papers are not able to support this.

For proceeding doses, we see that the *cc* plateaus yet the *cpl* decreases. In reference to the *cc*, it may be due to the clusters formed are more “isolated,” leading to groups which are far away that connections do not meet the net threshold set, and the surviving members are only those which are close to each other which decreases the *cpl*.

4.4.3 Small world coefficient (sw)

Upon completion of the determination of the *cc* and *cpl*, the small-world coefficient quantifies a network’s small-world property by comparing its clustering and path length to a random graph, which was of the Erdős-Rényi type. The graph portrays a trend that the *sw* increases before dose ~ 8 Gy (aggressive) and 10 Gy (slowly proliferating) which then decays at higher doses.

This trend of increase before the aforementioned doses is consistent with studies conducted, which foretell high values of small-world-ness with higher dose (up to 10 Gy) [5]. However, at even higher doses, as the graph suggests, small-world-ness decreases. This is due in part to the resulting fragmentation patterns that are displayed among the graphs in this paper, (Fig. 4a, 4b, 5a, 5b, 6a, 6b,). The trends paint a story of what can happen upon varying doses, which will be explained in the latter part of this section.

4.5 Morphological Effects of Radiation

Lastly, this study examined the individual physical effects of radiation on the cells themselves based on the simulation. At the very start, as observed from the previous graphs, the cells are clustered together, lessening its eccentricity as packing occurs. Increasing the dose, which led to eventual cell death, provided space for the cells to reform into geometries with higher eccentricity, eventually peaking at around 8 Gy (aggressive) and 10 Gy (slowly proliferating), after which, the eccentricity dropped. This implies the large, spread-out network has shattered into small, compact clusters. The “survivors” are no longer part of a wide-reaching colony; they are isolated in tiny, low-eccentricity islands.

The cell area keeps a decreasing trend as dose is increased. This may be due to decreased clustering as a result of fragmentation upon radiation application. The cluster (denoted by the large black region on the graph) at higher doses fragments while some of the cells die, continuously decreasing the area.

The perimeter first presents an increase before decreasing. At the stages where the perimeter increases, fragmentation increases the perimeter as disconnected cells contribute to the overall perimeter. However, higher doses increases the likelihood of cell death in comparison to fragmentation, leading to a drop in perimeter as well.

The mean roundness, related to the eccentricity, has low values at the start due to the clustering forming irregularities on the surface of the cells. This eventually reaches its minimum where fragmentation eventually starts, and roundness begins to form (along with eccentricity). At higher doses, cells tend to retract their shapes (thus forming the minimum surface area, similar to surface tension). An increase in roundness often signals a loss of migratory capacity and the onset of cell death.

4.6 The Big Story

The provided data from different dose applications provides a case-by-case basis on a series of events that may happen when applying low to high doses of radiation.

1. At low doses (0~2 Gy for aggressive and 0-5 Gy for slowly proliferating cells), the tumor cells are whole, able to withstand small amounts of radiation and be able to repair itself and communicate with its neighbors, providing additional support to restore damaged areas affected by radiation.
2. At intermediate doses (2~8 Gy for aggressive and 5-10 Gy for slowly proliferating cells), the tumor mass starts to favor fragmentation, and tumor cells start to undergo apoptosis to where the cells cannot recuperate. Cell proliferation is halted, relying on clustering groups for support and establishing reliable connections with readily nearby clusters.
3. At high doses (>8 Gy for aggressive and >10 Gy for slowly proliferating cells), necrosis starts to be favored in comparison to apoptosis. The main cluster is fragmented less, as more cell death is incurred within the main body. Cell proliferation is halted, and what remains of cell clusters, some are too far away to establish connections with other clusters, with the only reliable connections reserved for clusters which, by chance, are close to each other (close densities).

The results of this paper indicate that the environment simulated by the created model is somewhat accurate compared to experimental setups published, as evidenced by similar trends observed in Tirinato [5], which provided the basis for this paper. It may not be the most robust model, but future researchers are recommended to improve upon the model to take into account. The results of this study remarks that:

1. Topology has the high potential to become an important part in consideration of planning involving radiotherapeutic treatment, as it could tailor to the individuality of the person and their makeup,

- allowing for more carefully thought out treatment options in hospitals and care facilities.
2. The model itself has the potential to provide a framework for machine learning/artificial learning projects, providing means for the project to become extended not only to cover what has been covered in this paper, but also take into consideration other variable factors such as dose rates and radiation energies.
 3. Opportunities for effective treatment planning for low-income areas is possible, as less expensive equipment is needed to assist in tailoring treatment regimes, provided that the model is revised to provide more accurate results.

This study, however, is limited in its capacity to include consideration for other important factors, such as that:

1. **Structure.** The model itself was only able to provide a 2D model of cells. Future researchers are recommended to explore options involving 3D cell models, one that could take into account complex geometries of clustering, cellular debris as a result of apoptotic and necrotic events, etc.
2. **Time Evolution.** The model was not able to explore allowing the cells themselves to time evolve, to determine if, truly, cell proliferation is halted during the radiation process, which was considered to be an instantaneous application.
3. **Other Radiation Types.** The paper was not able to explore other radiation types (particularly particulate radiation) which need separate considerations mentioned in this paper.

With this being said, future researchers are encouraged to revise the model to also take account the aforementioned limitations, as the consequences for doing so can revolutionize how we can improve the status of oncological treatment in the country, maybe even the world.

5 Conclusions and Recommendations

The study was able to provide a solid framework for a model that can (a) simulate cancerous tissue with the appropriate properties and (b) simulate photon bombardment and treatment of such cancerous tissue to see how it evolves with varying doses applied, whose results turned out to be similar to studies conducted in laboratories. It was able to effectively display different results depending on the doses, with remarkable effects to its morphology and topology. From the model, topological metrics were successfully calculated, whose results are interpreted to be similar to what happens in real laboratory experiments.

This implies that there is potential to consider topology in radiation dosage calculation and optimization.

Future researchers are recommended to explore the capabilities of the model to explore 3D geometries,

amend additional properties of tissues that can be crucial in consideration of radiotherapy, and add options for particulate radiations to be simulated in the model.

6 Appendix

The code files and figures are available in a Github repository. Access it [here](#).

References

- [1] F. Bray, M. Laversanne, H. Sung, J. Ferlay, R. L. Siegel, I. Soerjomataram, and A. Jemal, Global cancer statistics 2022: Globocan estimates of incidence and mortality worldwide for 36 cancers in 185 countries, *CA: A Cancer Journal for Clinicians* **74**, 229–263 (2024), ISSN 1542-4863.
- [2] (2023), <http://www.iaea.org/newscenter/news/what-is-radiation-therapy>.
- [3] F. Pagliari, M. Spadea, P. Montay-Gruel, A. Puspitasari-Kokko, J. Seco, L. Tirinato, A. Accardo, F. De Angelis, and F. Gentile, Nanotopography enhanced topological-cell-analysis in radiation-therapy, *Advanced Healthcare Materials* **14** (2025), ISSN 2192-2659.
- [4] L. Tirinato, V. Onesto, D. Garcia-Calderon, F. Pagliari, M.-F. Spadea, J. Seco, and F. Gentile, Human lung-cancer-cell radioresistance investigated through 2d network topology, *Scientific Reports* **12** (2022), ISSN 2045-2322.
- [5] L. Tirinato, V. Onesto, D. Garcia-Calderon, F. Pagliari, M.-F. Spadea, J. Seco, and F. Gentile, Human cancer cell radiation response investigated through topological analysis of 2d cell networks, *Annals of Biomedical Engineering* **51**, 1859–1871 (2023), ISSN 1573-9686.
- [6] S. J. McMahon, The linear quadratic model: usage, interpretation and challenges, *Physics in Medicine amp; Biology* **64**, 01TR01 (2018), ISSN 1361-6560.
- [7] X. S. Qi, Q. Yang, S. P. Lee, X. A. Li, and D. Wang, An estimation of radiobiological parameters for head-and-neck cancer cells and the clinical implications, *Cancers* **4**, 566–580 (2012), ISSN 2072-6694.
- [8] J. Z. Wang, M. Guerrero, and X. Li, How low is the / ratio for prostate cancer?, *International Journal of Radiation Oncology*Biology*Physics* **55**, 194–203 (2003), ISSN 0360-3016.
- [9] K. Śłosarek, M. Konopacka, J. Rogoliński, and A. Sochanik, Effect of dose-rate and irradiation geometry on the biological response of normal cells and cancer cells under radiotherapeutic conditions, *Mutation Research/Genetic Toxicology and Environmental Mutagenesis* **773**, 14–22 (2014), ISSN 1383-5718.
- [10] E. J. Hall and D. J. Brenner, The dose-rate effect revisited: Radiobiological considerations of importance in radiotherapy, *International Journal of Radiation Oncology*Biology*Physics* **21**, 1403–1414 (1991), ISSN 0360-3016.

- [11] J. E. Turner, *Atoms, radiation, and radiation protection*, Physics textbook (Wiley-VCH, Weinheim, 2010), 3rd ed., ISBN 9783527406067.
- [12] S. Keam, K. M. MacKinnon, R. A. D'Alonzo, S. Gill, M. A. Ebert, A. K. Nowak, and A. M. Cook, Effects of photon radiation on dna damage, cell proliferation, cell survival, and apoptosis of murine and human mesothelioma cell lines, *Advances in Radiation Oncology* **7**, 101013 (2022), ISSN 2452-1094.
- [13] H. Murad, Y. Alghamian, A. Aljapawe, and A. Madania, Effects of ionizing radiation on the viability and proliferative behavior of the human glioblastoma t98g cell line, *BMC Research Notes* **11** (2018), ISSN 1756-0500.
- [14] J. Liu, Y. Liu, T. Xie, L. Luo, C. Xu, Q. Gao, L. Shen, F. Wan, T. Lei, and F. Ye, Radiation-induced g2/m arrest rarely occurred in glioblastoma stem-like cells, *International Journal of Radiation Biology* **94**, 394–402 (2018), ISSN 1362-3095.
- [15] E. M. Strasser-Wozak, B. L. Hartmann, S. Geley, R. Sgonc, G. Böck, A. J. Oliveira Dos Santos, R. Hattmannstorfer, H. Wolf, M. Pavelka, and R. Kofler, Irradiation induces g2/m cell cycle arrest and apoptosis in p53-deficient lymphoblastic leukemia cells without affecting bcl-2 and bax expression, *Cell Death amp; Differentiation* **5**, 687–693 (1998), ISSN 1476-5403.
- [16] J. B. Little, Differential response of rapidly and slowly proliferating human cells to x irradiation, *Radiology* **93**, 307–313 (1969), ISSN 1527-1315.
- [17] M. Tubiana, The kinetics of tumour cell proliferation and radiotherapy, *The British Journal of Radiology* **44**, 325–347 (1971), ISSN 1748-880X.
- [18] J.-s. Wang, H.-j. Wang, and H.-l. Qian, Biological effects of radiation on cancer cells, *Military Medical Research* **5** (2018), ISSN 2054-9369.
- [19] C. F. Labuschagne, E. C. Cheung, J. Blagih, M.-C. Domart, and K. H. Vousden, Cell clustering promotes a metabolic switch that supports metastatic colonization, *Cell Metabolism* **30**, 720 (2019), ISSN 1550-4131.
- [20] B. Rath, A. Plangger, D. Moser, M. Hochmair, E. Ulsperger, and G. Hamilton, Protection of small-cell lung cancer circulating tumor cells by cellular fragmentation, *Journal of Cancer Metastasis and Treatment* **2020** (2020), ISSN 2394-4722.